Journal of Inorganic and General Chemistry
ZAAC
Zeitschrift für anorganische und allgemeine Chemie
www.zaac.wiley-vch.de
RESEARCH ARTICLE
DOI: 10.1002/zaac.202400074

Unraveling Strong Supramolecular Assembly of a Novel Pyrene Based Hg(II)-complex: Insights from Hirshfeld Surface, FMO and Molecular Electrostatic Potential (MEP) Analyses

Shibashis Halder,[a] Yeasin Sikdar,[b] Mohd Afzal,[c] Mridula Guin,*[d] and Saugata Konar*[b]

A rare pyrene-based coordination compound of Hg(II) $[Hg(L)_2]$ (**1**) (where, HL = 2-((Pyren-1-ylmethylene)amino)benzenethiol) was synthesized and characterized by single crystal X-ray diffraction (SC-XRD) analysis. Crystallographic analysis revealed that complex **1** has seesaw geometry with HL coordinated as a bidentate ligand to a metal ion. The role of weak forces like π···π and CH···π interactions in influencing the self-assembly process appears to be of importance. The electronic structure of the complex was predicted using DFT calculations with mixed basis set. DFT calculated structural parameters are in good agreement with the experimentally obtained parameters from XRD. Molecular reactivity and stability of the complex has been assessed through frontier molecular orbital analysis. Evaluation of molecular electrostatic potential (MEP) displays the electrophilic and nucleophilic reactivity sites. The Hirshfeld surface analysis clearly indicates C–H···π interactions and π···π stacking interactions are responsible to extend the supramolecular network of the complex. Analyses of the Finger print plots suggest that H···H and H···C contacts are major interactions for stabilizing the molecular crystal.

1. Introduction

Advancement in single crystal X-ray crystallography during the last two decades have greatly contributed in better understanding of supramolecular non-covalent interactions.[1–3] Crystal engineering's rapid expansion stems from a growing understanding of intermolecular interactions in solid-state structures.[4,5] Modern crystal engineering relies heavily on understanding intermolecular interactions and consequent solid-state formations.[6–8] So, supramolecular chemists often emphasize weaker interactions that can significantly alter the spatial arrangement of dominant structural motifs. In addition to this, designing and development of heavy metal ion-based coordination complexes, which can exhibit fascinating structural architecture and unique non-bonding interaction, are extremely important for the researchers in the field of both coordination chemistry as well as crystal engineering.

We have been actively investigating well defined weak interactions for the last five years, using both theoretical and experimental methods. Thus, we have tried and established beyond a shadow of a doubt their crucial role in the solid-state packing of 3d transition metal-based hybrid inorganic-organic materials. In this context, extensive research based on mercury (5d transition metal) based coordination complex has been conducted with special emphasis on π···π interactions in solid-state networks, highlighting their significance as weak stabilizing forces in molecular structure containing pyrene-based ligand. Till now crystal structures (obtained from single crystal X-ray diffraction analysis) of Hg(II) complexes with pyrene-based ligands are very rare. Gervasio *et al.* reported "mercury as a receptor of pyrene".[9] They were able to isolate the crystal and reported the single crystal X-ray diffraction data. As reported there existed weak interaction between the Hg(II) centre and the carbon atoms of the pyrene ring. To the best of our knowledge no others crystal structures of pyrene based Hg(II) complex have been reported till date. Although there are numerous Hg^{2+}-ion sensors based on pyrene moiety and the authors also claimed about the formation of complexes during the sensing experiments but there is no instance of their isolation and formation of crystal, and thereafter obtainment of crystal structure from single crystal X-ray diffraction analysis. This result encouraged us to synthesize a novel pyrene based Hg(II) complex and to study its solid state geometry thereby getting into different kinds of interactions existing within the molecular architecture. Also, we focused to study the possible

[a] *S. Halder*
Department of Chemistry
T.N.B. College
Bhagalpur, Bihar 812007, India
[b] *Y. Sikdar, S. Konar*
Department of Chemistry
The Bhawanipur Education Society College
Kolkata 700020, India
E-mail: Saugata.konar@gmail.com
[c] *M. Afzal*
Department of Chemistry
College of Science
King Saud University
Riyadh 11451, Saudi Arabia
[d] *M. Guin*
Department of Chemistry and Biochemistry
Sharda University
Greater Noida, Uttar Pradesh 201310, India
E-mail: mridula.guin@sharda.ac.in

Supporting information for this article is available on the WWW under https://doi.org/10.1002/zaac.202400074

CH···π interactions since they can serve as pivotal organizing factors to create supramolecular structure.

Additionally, DFT calculations help to understand non-covalent interactions such as electrostatic force, hydrogen bonding, π···π, CH···π and Van der Waals interactions. These interactions serve as the primary forces in supra molecular architecture formation.[10,11] DFT calculations can accurately predict molecular geometry, interaction energy, and supramolecular system stability. Also, Hirshfeld surface analysis, fingerprint plots, and 3D energy framework analysis can reveal supramolecular themes inside a molecular structure. This study used DFT calculations to analyze the electronic structure, molecular electrostatic potential (MEP), and frontier molecular orbitals (FMO). Hirshfeld surface analysis is used to analyze intermolecular interactions and surface features in molecular crystals.

In the current communication, we present our attempt to synthesis a crystal structure of rare pyrene-based Hg(II) complex **1**. To the best of our knowledge, it is the first reported compound of pyrene-based seesaw shaped Hg(II) complex. This observation makes our study more relevant since our main focus is to elucidate the solid-state structure as well as the various types of weak interactions. We have shown supramolecular extended architectures generated by means of π···π and CH···π interactions in **1** which were examined carefully and described in detail. DFT computations were used to analyze the electronic structure, electrostatic potential (MEP), and frontier molecular orbitals (FMO). Furthermore, Hirshfeld surface analysis was used to better understand the crystal packing and the various forms of intermolecular interactions that contribute to molecular crystal stability. Crystal structure explores how ligand molecules influence the geometry of the metal centre. Without crystal structure it is impossible to determine actual geometry around the metal centre. With the crystal structure, we have determined the seesaw geometry around Hg(II) centre. The pivotal objective of this work includes elucidation of the structural characteristics of the pyrene-based Hg(II) complex which can be classified under rare complex category (seesaw shaped). Investigation of the various weak interactions within the solid-state crystal of the synthesized complex and theoretical studies to justify these observations provide new dimensions to this work. We sincerely hope that this study should become greatly significant to the researchers working on molecular designing and crystal engineering.

Experimental Section

Materials and Measurements

All reagents and chemicals were of AR grade and obtained from commercial sources (SD Fine Chemicals and Aldrich) and used without further purification. Elemental analyses (C, H and N contents) were carried out by a Perkin-Elmer CHN analyzer 2400. IR spectra were recorded in the region of 4000–400 cm^{-1} using a Perkin-Elmer model 883 infrared spectrophotometer.

Synthesis of Ligand HL

The Ligand HL is synthesized according to the literature method.[12] IR (KBr pellet/cm^{-1}): 3131, 2947, 2660, 1635, 1577, 1487, 768.

Synthesis of Complex 1

Complex **1** was synthesized by refluxing a methanolic solution containing 1 mmol (0.342 g) of $Hg(NO_3)_2 \cdot H_2O$ and 2 mmol (0.334 g) of HL for nearly 5 h. The solution thereafter was cooled to room temperature and filtered. Yellow colored needle shaped crystals were obtained by slow evaporation of the reaction mixture at room temperature. (Yield: 67 %). M. P. (°C) = > 300. Elemental analysis: anal. calc. for $C_{46}H_{28}HgN_2S_2$: C, 63.20; H, 3.21; N, 3.21; Found: C, 63.18; H, 3.20; N, 3.23 %. IR (KBr pellet/cm^{-1}): 1623, 1544, 1446, 626.

Crystallographic Data Collection and Refinement

Selected crystal data for **1** is given in Table 1. Data collections were made using Bruker SMART APEX II CCD area detector equipped with graphite monochromated Mo Kα radiation (λ = 0.71073 Å) source in ω scan mode at 293(2) K for both. Cell parameters refinement and data reduction were carried out using the Bruker SMART APEX II. Cell parameters refinement and data reduction were carried out using Bruker SMART[13] and Bruker SAINT softwares. The structure of the complex was solved by conventional direct methods and refined by full-matrix least square methods using F2 data. SHELXS-97 and SHELXL-97 programs[14] were used for structure of complex solution and refinement respectively.

Density Functional Theory (DFT) Study

All quantum chemical calculations are carried out using Gaussian 16 program package[15] and the visualization was performed through Gauss View 6.0 program.[16] The ground state geometry of the complex was determined using DFT calculation by B3LYP

Table 1. Crystal data for Complex **1**.

Formula	$C_{46}H_{28}N_2S_2Hg$
Formula weight	873.41
Crystal system	Monoclinic
Space group	P 21/c
a/Å	7.0667(2)
b/Å	28.2372(8)
c/Å	18.5467(5)
α/°	90.00
β/°	98.5780(10)
γ/°	90.00
V/Å^3	3659.48(18)
Z	4
D_c/g cm^{-3}	1.585
μ/mm^{-1}	4.356
F(000)	1720
θ range/°	1.32–27.91
Reflections collected	60576
Unique reflections	8641
Reflections $I > 2\sigma(I)$	4637
R_{int}	0.1490
Goodness-of-fit (F^2)	0.944
R_1 ($I > 2\sigma(I)$)[a]	0.0605
wR_2[b]	0.1252
$\Delta\rho$max/min/e Å^3	-0.79, 0.67

[a] $R_1 = \Sigma||F_o| - |F_c||/\Sigma|F_o|$, [b] $wR_2 = [\Sigma(w(F_o^2 - F_c^2)^2)/\Sigma w(F_o^2)^2]^{1/2}$.

function[17,18] along with mixed basis set of 6-31+G* for all atoms except Hg atom for which effective core potential LANL2DZ basis set was utilized. The DFT/B3LYP function is known for accurate prediction of molecular structure and charge densities in transition metal complexes. The convergence criteria were maintained at default level without any constraint on the geometry. Absence of imaginary frequency during vibrational frequency calculation, confirmed the optimized geometry as true minima on the potential energy surface. Energies of HOMO (Highest Occupied Molecular Orbital), LUMO (Lowest Unoccupied Molecular Orbital) and band gap are determined to understand the chemical reactivity of the compound. Moreover, molecular electrostatic potential of the compound is calculated from the electron density to predict the electrophilic and nucleophilic regions in the complex.

Molecular Hirshfeld Surface Analysis

Hirshfeld surface analysis is an important tool to understand crystal packing and intermolecular interactions in a molecular crystal. The intermolecular close contacts can be visualized qualitatively and quantitatively through the Hirshfeld surface. The red-white-blue coloured surface of the normalized contact distance *d*norm identifies the close contacts around van der waals radius, short contacts and long contacts. The mapped *d*norm surface shows red spots wherever close contacts are present in the molecular crystal.

Crystal Explorer 17.5 program[19] is used to perform Hirshfeld surface (HS) analysis of the complex using the cif file. Three colour coded surface e.g. *d*norm, shape index and curvedness were mapped for the molecular crystal. The Hirshfeld surface was generated using a high standard surface resolution. All the surfaces were presented in a transparent mode for clear visualization. Additionally, 2D finger-print plots in terms of d_e and d_i are determined to summarize the nature and type of intermolecular contacts used in packing of the molecular crystal.

2. Results and Discussion

2.1. Structural Description of Complex 1

SC-XRD reveals complex **1** as a mononuclear entity consisting of one Hg(II) ion chelated by two monoanionic ligands having sp^2 N and S donor atoms as depicted in Figure 1. The bond distances and bond angles around metal centre are tabulated in Table 2 with close conformity with other published HgN_2S_2 core. The imine N atom and thiophenoxo S atom from both the ligands chelate the metal centre where the phenyl rings are *trans* to each other and the electron rich pyrene rings are *cis* to each other having extensive intramolecular π···π interaction (*vide infra*) leads to dihedral angle between the planar phenyl ring and pyrene ring to 65.07° and 55.44°. To infer the coordination geometry around Hg(II), the visual inspection shows the geometry to be see-saw (S1 and S2 in nearly same plane,165.64(7) and N1 and N2 below (equatorial), 103.95(16)) where the two largest trans angles are 165.64(7)° and 114.36(13)°. The Hg–S and Hg–N bond distances are in accordance with HgS_2N_2 coordination environment. S1 and S2 sulphur atoms are distanced from the HgS_2N_2 mean plane by 0.837 and 0.849 Å respectively while N1 and N2 are displaced by 1.108 and 1.125 Å from HgS_2N_2 mean plane respectively. We have also calculated the geometry index for four-coordinate

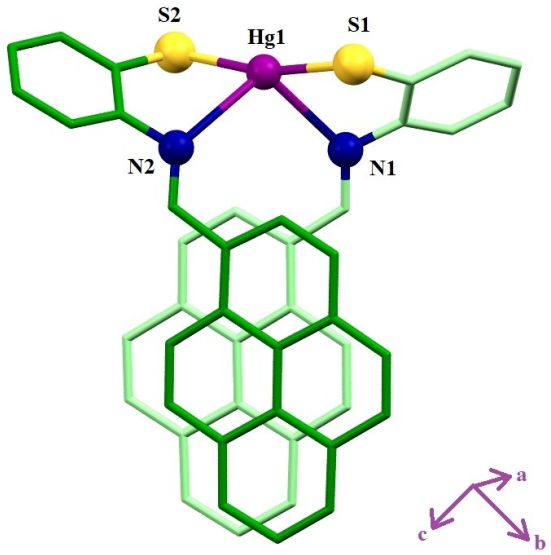

Figure 1. Molecular structure of Complex **1** with partial atom numbering. H-atoms are removed for clarity.

Table 2. Selected bond lengths (Å) and selected bond angles (°).

Hg1–S1	2.355(2)
Hg1–S2	2.362(2)
Hg1–N1	2.700(6)
Hg1–N2	2. 704(5)
S1–Hg1–S2	165.64(7)
S1–Hg1–N1	75.27(13)
S2–Hg1–N1	114.36(13)
S1–Hg1–N2	114.24(12)
N1–Hg1–N2	103.95(16)
S2–Hg1–N2	74.88(12)
C40–S1–Hg1	101.2(3)
C46–S2–Hg1	101.6(2)
C33–N1–Hg1	135.2(5)
C35–N1–Hg1	103.8(4)

Table 3. Continuous Shape Measures (CShMs) of Hg-centres relative to ideal 4-vertex polyhedra. The lowest CShMs value which corresponds to closest geometry is highlighted in bold.

	Hg1	Symmetry	Ideal shape
vTBPY-4	21.26	C_{3v}	Vacant trigonal bipyramid
SS-4	16.211	C_{2v}	Seesaw
T-4	23.059	T_d	Tetrahedron
SP-4	16.68	D_{4h}	Square

complexes, τ_4 as proposed by Yang *et al.*[20] by following equation:

$$\tau_4 = \frac{360^0 - (\alpha + \beta)}{141^0}, \quad (1)$$

where α and β are the two largest angles in the four-coordinate geometry of the complex. For a perfect tetrahedral and square planar geometry τ_4 has the values of 1 and 0 respectively. The

Table 4. π···π interaction in complex **1**.

C_g(ring)···C_g(ring)	C_g···$C_g$distance(Å)	Slippage(Å)	Type	Symmetry for equivalent atoms
$C_g(3)$···$C_g(7)$	3.984(4)	3.528	Intramolecular	
$C_g(3)$···$C_g(7)^{\#}$	4.072(4)	3.478	Intermolecular	#: 1 + X,Y,Z
$C_g(3)$···$C_g(8)^{\#}$	4.014(4)	3.525	Intermolecular	#: 1 + X,Y,Z
$C_g(4)$···$C_g(7)$	3.937(4)	3.505	Intramolecular	
$C_g(4)$···$C_g(8)$	3.564(4)	3.489	Intramolecular	
$C_g(4)$···$C_g(8)^{\#}$	3.568(4)	3.526	Intermolecular	#: 1 + X,Y,Z
$C_g(5)$···$C_g(9)$	3.973(4)	3.495	Intramolecular	
$C_g(5)$···$C_g(9)^{\#}$	4.166(4)	3.525	Intermolecular	#: 1 + X,Y,Z
$C_g(6)$···$C_g(8)$	3.969(4)	3.491	Intramolecular	
$C_g(6)$···$C_g(8)^{\#}$	4.126(4)	3.522	Intermolecular	#: 1 + X,Y,Z
$C_g(7)$···$C_g(3)$	3.985(4)	3.528	Intramolecular	
$C_g(7)$···$C_g(4)$	3.938(4)	3.489	Intramolecular	

Ring number of centroid:
Cg(3):C(1)→C(2)→C(3)→C(15)→C(13)→C(14);Cg(4):C(3)→C(4)→C(5)→C(6)→C(16)→C(15);
Cg(5):C(6)→C(7)→C(8)→C(9)→C(10)→C(16); Cg(6): C(10)→C(11)→C(12)→C(13)→C(15)→C(16)
Cg(7):C(17)→C(18)→C(19)→C(31)→C(29)→C(30); Cg(8): C(19)→C(20)→C(21)→C(22)→C(32)→C(31)

Table 5. C–H···Cg (π ring) interaction in complex **1**.

C–H···C_g	H···C_g(Å)	H-Perp(Å)	X–H···C_g(°)	X···C_g(Å)	Symmetry for equivalent atoms
C(11)–H(11)···Cg(11)[a]	2.87	2.749	156	3.741(9)	a: X,1/2-Y,1/2 + Z
C(14)–H(14)···Cg(12)[b]	2.75	2.742	155	3.615(9)	b: 1 + X,1/2Y,1/2 + Z
C(39)–H(39)···Cg(12)[c]	2.89	2.801	144	3.691(8)	c: X,1/2-Y,−1/2 + Z

Cg(11):C(35)→C(36)→C(37)→C(38)→C(39)→C(40)
Cg(12):C(41)→C(42)→C(43)→C(44)→C(45)→C(46)

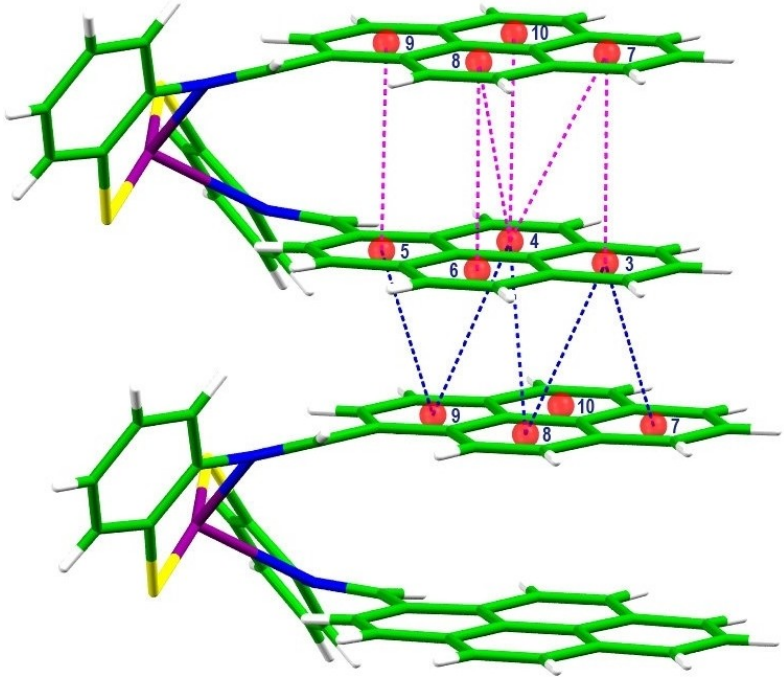

Figure 2. Various intermolecular (shown in blue) and intramolecular (shown in magenta) π···π stacking interaction in the 1-D chain along crystallographic axis *a*. (C_g···C_g distance limited to < 4.1 Å). Cg (ring number) is mentioned inside the individual six membered ring.

less common four coordinate geometry like trigonal pyramidal and see-saw falls within the range of 0 and 1. Table S1 depicts some four coordinated mercury complexes with reported see-saw geometry where four-coordinate geometry index τ_4 which

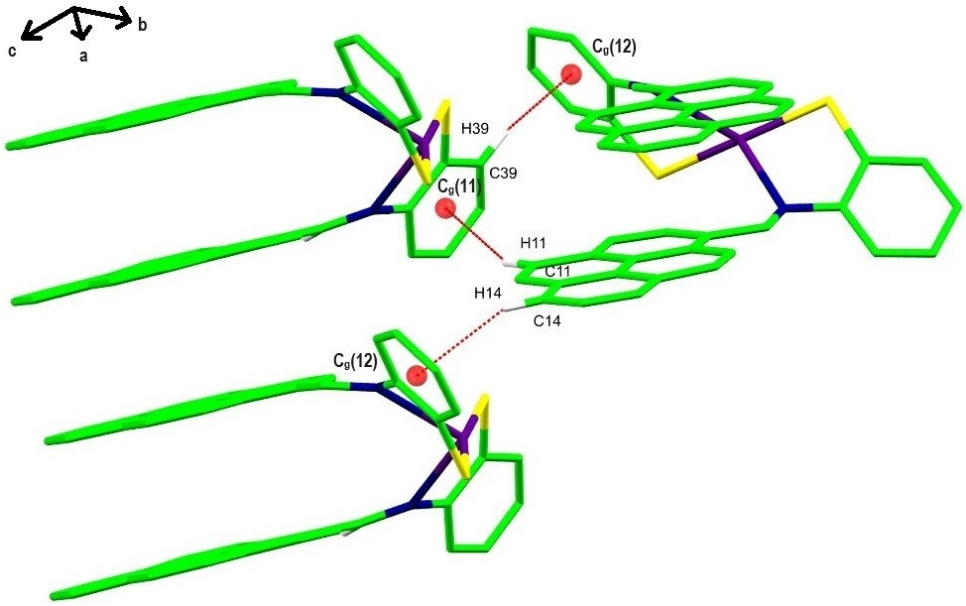

Figure 3. C–H···π interaction between the 1-D chain in complex **1**.

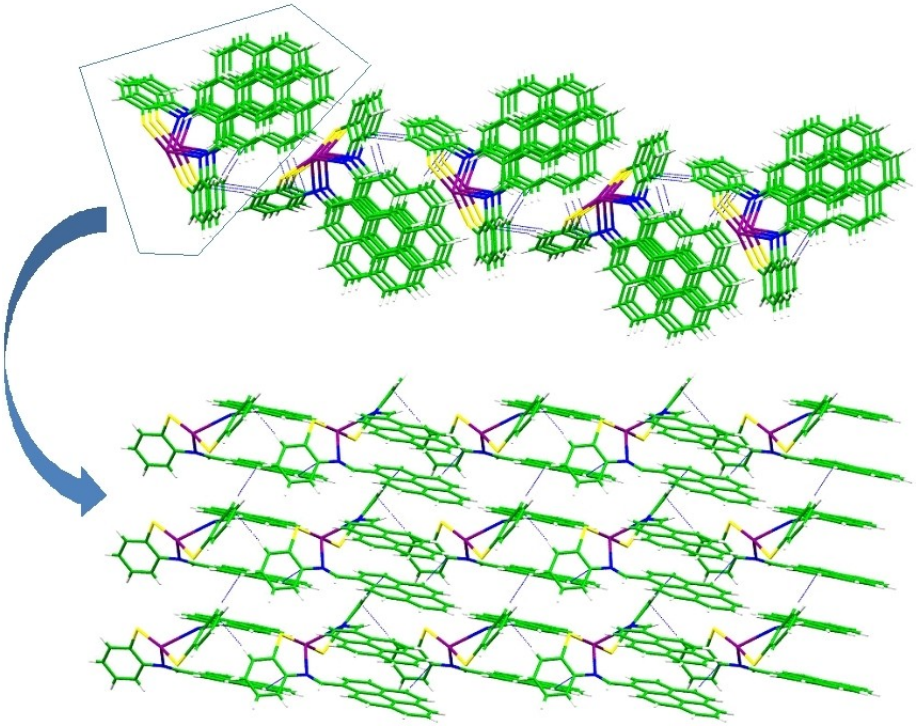

Figure 4. Depiction of formation of 2-D sheet in complex **1**. Dotted blue lines are the C–H···π interactions between the 1D- strand.

shows mostly see-saw complexes has τ_4 value in the range of 0.56–0.84. Only the entry 5 of Table S1 formulated as [Hg-(18S4O2)]$(ClO_4)_2$ [21] (where, 18S4O2 represents 1,10-dioxa-4,7,13,16-tetrathiacyclooctadecane) has τ_4 value of 0.61 but the geometry was reported as distorted tetrahedral where the S–Hg-S bond angle ranges from 85.96° to 138.96°, but the median value was close to an ideal tetrahedral value of 110.04°. So, prediction of see-saw geometry from τ_4 value needs more examples for generalization.

For more conformity of coordination geometry, we performed Continuous Shape Measurement for ML_4 geometry where the lowest CShMs value corresponds to Seesaw (C_{2v})

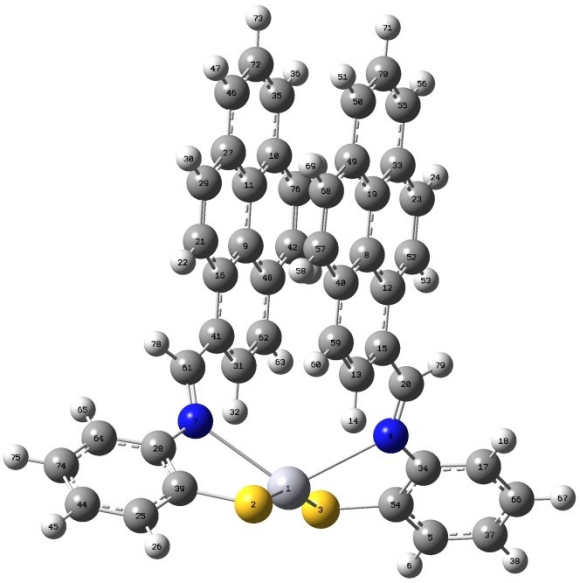

Figure 5. DFT optimized structure of the Complex **1**.

Table 6. FMO energy parameters and global reactivity descriptors of the complex **1.**

Parameters	Values (eV)
HOMO (eV)	−5.345
LUMO (eV)	−2.578
ΔE = (LUMO-HOMO) (eV)	2.767
$I = -$E(HOMO)(eV)	5.345
$A = -$E(LUMO) (eV)	2.578
$\chi = (I + A)/2$ (eV)	3.961
$\mu = -\chi$ (eV)	−3.961
$\eta = (I - A)/2$ (eV)	1.383
$S = 1/\eta$ (eV)	0.723
$\omega = \mu^2/2\eta$ (eV)	5.672

geometry (See Table 3 for details of Continuous Shape Measures calculation). One point to note that high CShMs value of see-saw (C_{2v}) geometry signifies considerable deviation from ideal geometry.[22]

Complex **1** contains extensive range of C–H···π and π···π stacking interactions in its supramolecular structure which yield infinite 2-dimensional sheet along crystallographic axes *a* and *c*. First, along axis *a* individual molecules are connected to form infinite 1-D chain stabilized by various flipped-parallel π···π stacking interaction of slippage < 3.6 Å (Table 4 and Figure 2). These individual 1-D chains are stitched by means of C–H···π interaction to form infinite 2-dimensional sheet (Table 5 and Figure 3). Thus, the coalescence of intra and intermolecular π···π stacking and C–H···π interactions between the 1-D strands leads to the formation of infinite 2-dimensional sheet along with *cis* orientation of the pyrene moiety (Figure 4).

2.2. Infrared Spectral Studies

The IR spectra of both the free ligand (HL) and complex **1** were recorded (Figure S1 and S2 respectively). The IR spectrum of the ligand (HL) can be compared with that of the complex to study the structural changes in the ligand upon complexation. The ligand exhibits a band at 3131 cm^{-1} which can be attributed for pyrene ring =C–H group. The free ligand also shows a IR stretching band at 2660 cm^{-1}due to the presence of SH moiety. A significant change in the C–S stretching frequency can be observed upon formation of the complex. For the free ligand it can be observed at 768 cm^{-1} and upon complexation it is shifted to 626 cm^{-1}. Similarly, the pyridyl CH=N stretching frequency is observed at 1635 cm^{-1} for the free ligand and upon complexation this band shifted to a lower wave number 1623 cm^{-1}. In HL, the IR bands positioned at 2947 cm^{-1}, 1577 cm^{-1} and 1487 cm^{-1} can be attributed to aromatic C–H bending, C–C stretching and aromatic C=C stretching (within the ring), respectively. Whereas, for **1**, the IR bands for the C–C stretching and aromatic C=C stretching (within the ring) can be observed at 1544 cm^{-1} and 1446 cm^{-1}, respectively.

2.3. Geometry from DFT Calculation

The optimized geometry of the complex is shown in Figure 5. The optimized structural parameters along with the experimental crystallographic data of the molecule arelisted in Table S2. The data clearly indicate that the computed bond distance and angles are in good agreement with the experimental geometrical parameters obtained from X-ray crystallography. The complex acquires a distorted tetrahedral geometry (seesaw geometry) around the Hg atom. The four donor sites around the central metal atom are shared by two imine N atoms and two thiophenoxo S atoms from the two ligand fragments. The two pyrene rings are in parallel plane with each other separated by about 5.2 Å while the two phenyl rings arranged in trans position. (∠S2-Hg1-S3 = 160.3). The bond angles of donor atoms with the central metal atom Hg are calculated as ∠S2-Hg1-S3 = 160.13, ∠N7-Hg1-N4 = 117.64, ∠S2-Hg1-N7 = 73.90, ∠S2-Hg1-N4 = 117.18, ∠S3-Hg1-N7 = 117.01, and ∠S3-Hg1-N4 = 73.95. Both the Hg–N bond distances are almost similar while the Hg–S bond lengths differ slightly by about 0.002 Å. These calculated structural parameters are in accordance with the parameters obtained from XRD, establishing the capabilities of DFT to predict the structure quite accurately.

2.4. Frontier Molecular Orbital (FMO) Analysis

The frontier molecular orbital analysis was performed to determine the global reactivity descriptors for a comprehensive understanding of reactivity and stability of the compound. The energy gap between frontier molecular orbitals (HOMO and LUMO) of a molecule is an important parameter to predict the stability and reactivity of the system. Various quantum chemical descriptors such as ionization potential (I) and electron affinity (A), global

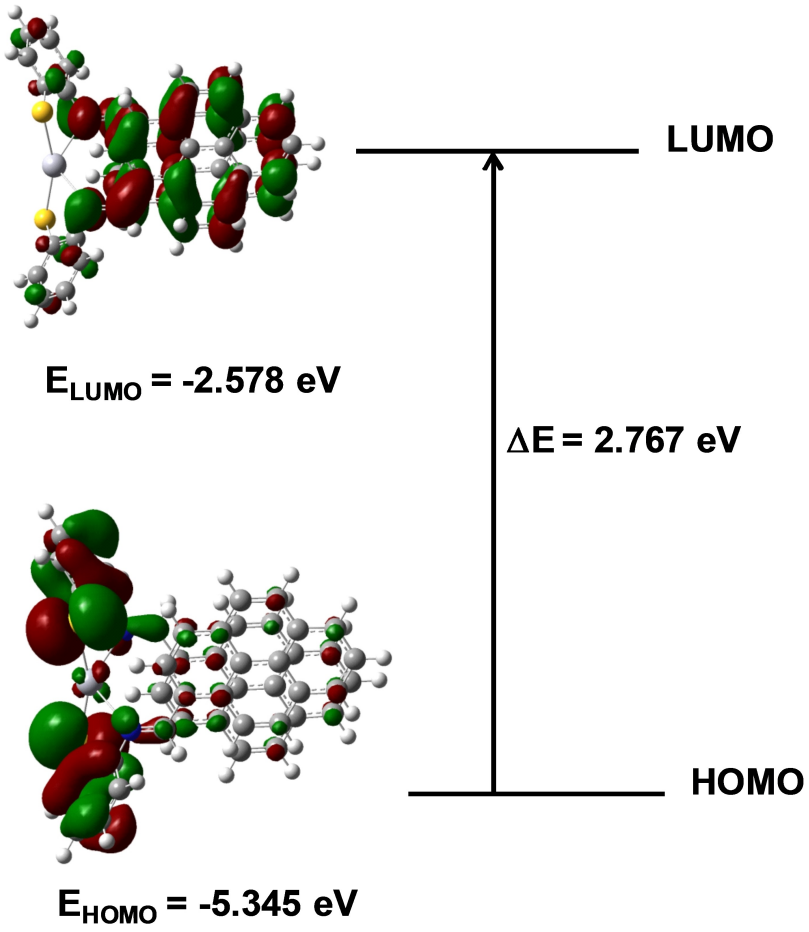

Figure 6. 3D surface plots of HOMO and LUMO of the Complex **1**.

hardness (η), global softness (S), electronegativity (χ), chemical potential (μ) and electrophilicity index (ω) of the molecule are computed and summarized in Table 6. The ionization potential measures the energy required to remove an electron from HOMO. The high value of I (5.345 eV) indicates significant ability of the compound to donate electrons. The electron affinity is the amount of energy change in the process of electron addition in the LUMO. Electron affinity of 2.578 eV signifies a decent ability of the compound for electron acceptance. Electronegativity (χ) represents how strongly it attracts electrons towards it. χ value of 3.961 shows considerable power of the compound to attract electrons. Global hardness (η) and chemical potential (μ) are related to the stability of the compound. The chemical hardness 1.383 eV shows resistance to change the electronic charge distribution imparting stability of the compound. The chemical potential −3.961 measures the intrinsic tendency of the compound to exchange electrons with the environment. Chemical softness is the inverse of hardness and directs the ease of deformation of electron cloud. The softness 0.723 signifies the compound to be less soft that means it is relatively hard, supporting the hardness value. The electrophilicity index (ω) indicates the propensity of the compound to accept electrons. The high value of 5.672 indicates the compound to show significant electrophilicity. The computed FMO surface plots of HOMO and LUMO is displayed in Figure 6. The LUMO is mostly localized over the pyrene rings while the HOMO is distributed over the thiophenoxo groups. The low band gap (2.767 eV) predicts the molecule to be more polarized, kinetically less stable and chemically reactive. There will be facile charge transfer process in the molecule due to low band gap. Again, the chemical hardness and softness along with the chemical potential and electrophilicity index value support the high reactivity of the molecule to alter the electron density. Table S3 shows a comparative study of the band gaps of some previously reported tetra-coordinated Hg(II)-complexes compared with **1**.

2.5. Molecular Electrostatic Potential (MEP)

The electrostatic potential of a molecular entity is a valuable tool to predict electrophilic and nucleophilic sites within the molecule. The propensity of formation of various types of intermolecular interactions for example, hydrogen bonding, drug-receptor interaction, enzyme-substrate interactions etc. is majorly based on the electrostatic potential of the molecule.[23] The MEP of the complex is calculated using electron density of

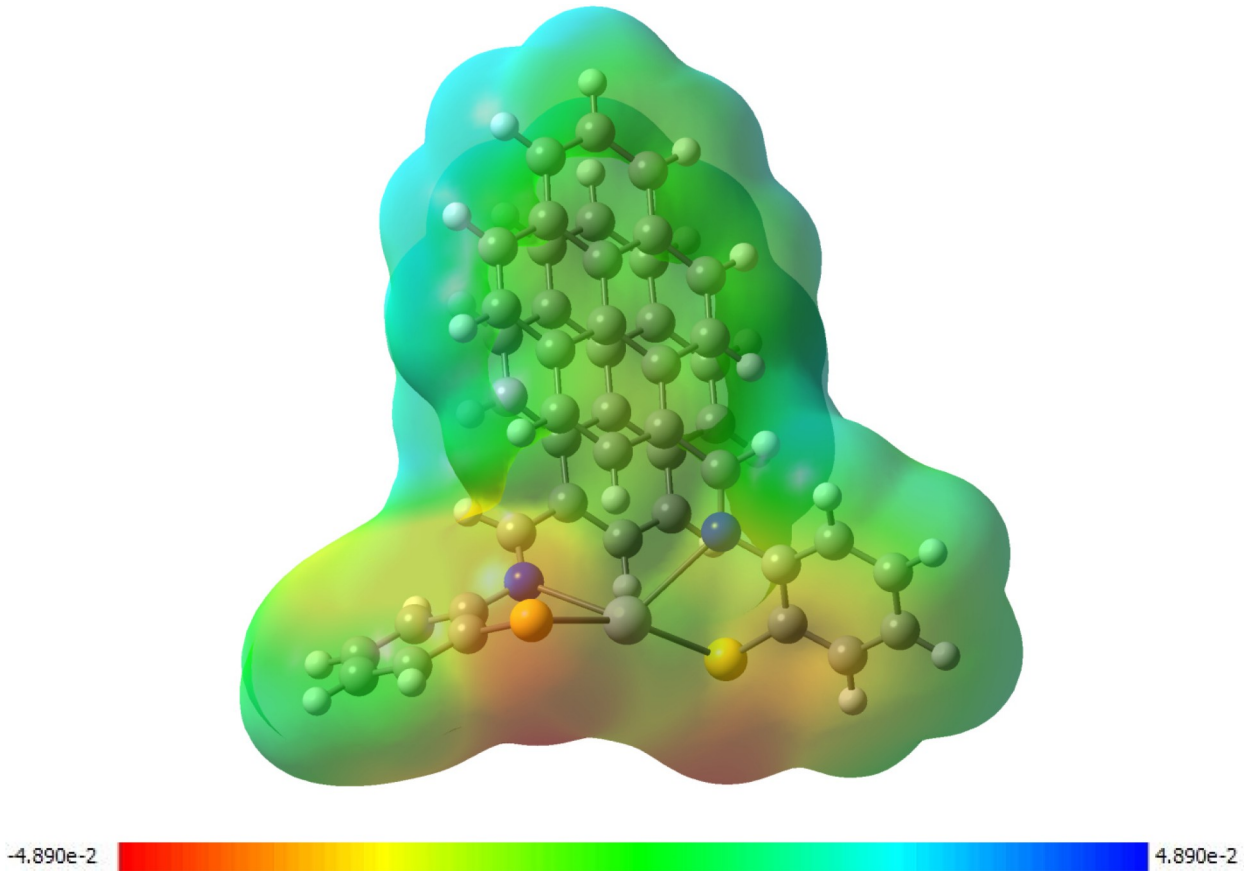

Figure 7. Molecular electrostatic potential map of the Complex **1**.

the optimized structure and displayed in Figure 7. The 3D map highlights the electron density in terms of different colour in increasing order blue < green < yellow < orange < red. The figure indicates the molecules mostly as neutral. However, presence of high electron density or negative charge is observed around the donor sulfur atoms near the metal centre (orange-red colored surface). The area around the hydrogen atoms of the pyrene rings displays bluish colour indicating electron deficiency. Thus, the electrophilic reactivity of the complex will be centered around the pyrene rings whereas nucleophilic reactivity around the thiophenoxo group near the sulfur atoms of the molecule.

2.6. Hirshfeld Surface Analysis

The Hirshfeld surfaces of the compound mapped in terms of *d*norm, curvedness and shape index are shown in Figure 8. The *d*norm surface represents the normalized contact distance. Small, dull red spots in the *d*norm surface indicates the atoms present in close proximity to the inner and outer side of Hirshfeld surface arising due to the weak CH···π, π···π and CH···C interactions (Figure 8a). The white and blue surfaces indicate atoms with medium proximity and large distance respectively from the Hirshfeld surface. The red spots are marked with the associated inter and intramolecular interactions involved to build the supramolecular self assembly of the compound is shown in Figure 8b. The red spot marked with π···π interaction arises due to the intramolecular π···π stacking interaction between two adjacent pyrene rings. The red spot for CH···π interaction is an intermolecular interaction formed due to the interaction between C–H group of a pyrene fragment of a molecule with the π cloud of the phenyl ring of the other molecule. Further a red spot due to CH···C intermolecular interaction is also observed due to the interaction between C–H group of a phenyl ring of a molecule with the carbon atom of a pyrene ring of another molecule. The size of all these spots is small and intensity of red colour is very low signifying the weak nature of these interactions. The shape index and curvedness determine the shape and surface area of the molecule. The shape index is a key parameter in understanding the presence of π···π stacking interactions in the packing modes of the crystal.[24] The shape index surface (Figure 8c) shows adjacent red and blue triangles marked with a circle indicating the presence of adjacent concave and convex region. This implies that the molecular crystal is stabilized with π–π stacking interactions. Further the curvedness map (Figure 8d) supports the findings of shape index. The presence of large flat surface patches in the curvedness map clearly tells that the crystal is packed with planar π···π stacking interactions.

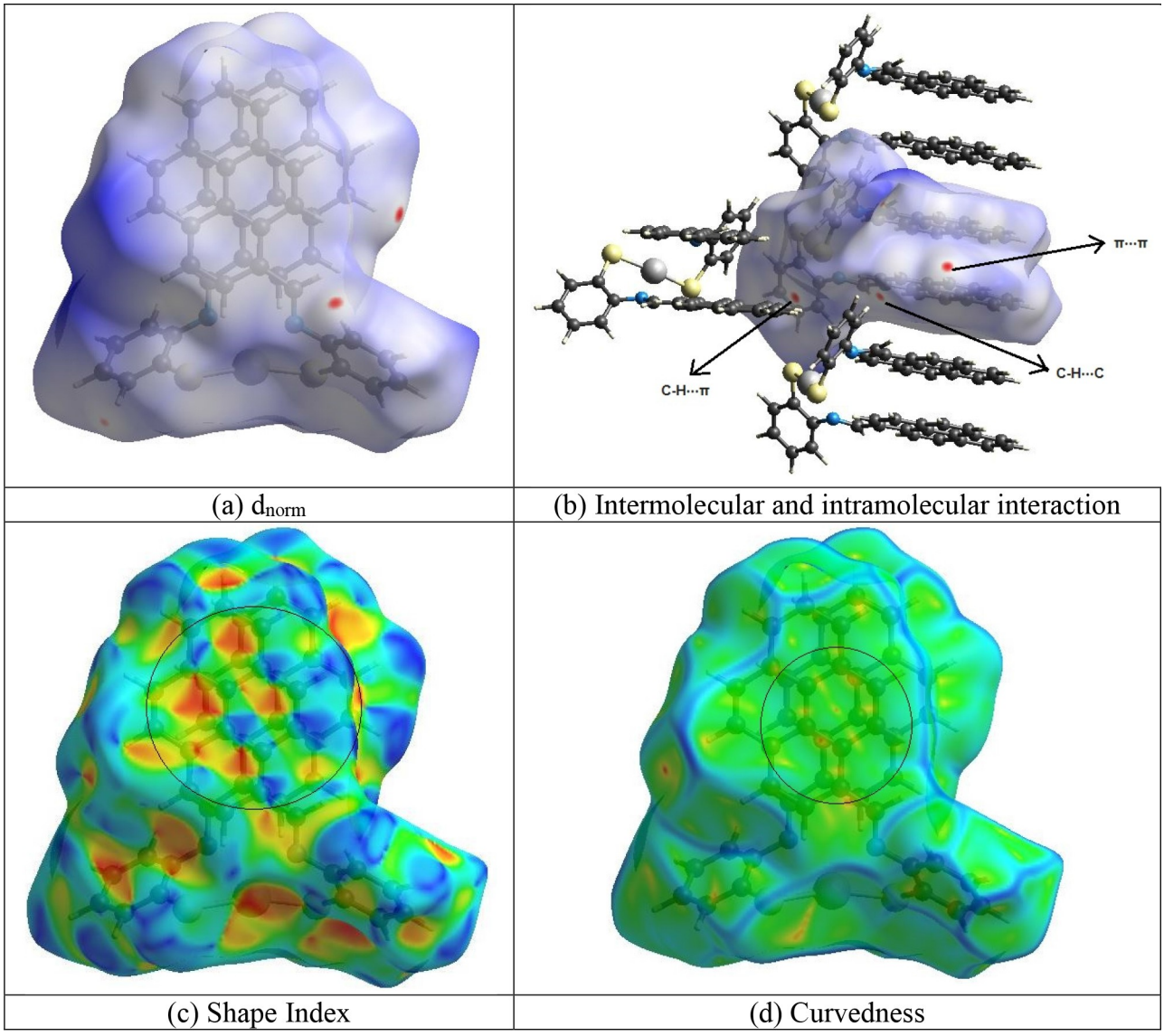

Figure 8. Hirshfeld surfaces mapped over (a) d_{norm}, (b) intermolecular and intramolecular interactions (c) shape index and (d) curvedness.

The two-dimensional fingerprint plots (Figure 9) of the major contacts are determined to quantify the intermolecular interactions. The molecular crystal is mostly packed with H···H and C···H contacts as major interactions contributing about 51.7% and 24.7% respectively to the overall crystal packing. The C···H contacts display characteristics wing feature with bow-tie pattern confirming the presence of π–π stacking interactions and C–H···π interaction in the crystal.[25–28] Additionally, N···H and S···H contacts are also observed stabilizing the crystal through weak hydrogen bonding interaction. S···H contacts are observed with feeble symmetrical sharp spikes however N···H contacts in the FP plots are noticed without their signature symmetrical sharp spikes confirming the weak nature of S···H intermolecular interactions.[29] Other significant interactions with minor contribution in the crystal packing are Hg···H, contributing 3.2% to the packing of the crystal.

3. Conclusions

Herein, we have designed and developed a Hg(II) based coordination compound with intriguing structural architecture. Non-covalent interactions such as π···π and CH···π are crucial for forming an extensive network in the synthesized metal complex framework. The DFT optimized structure of the complex is in good agreement with the structure obtained from X-ray crystallography having seesaw geometry. Various reactivity descriptors calculated from the FMO analysis predicts the complex to be chemically stable and reactive. The Hirshfeld surface investigation demonstrates H···H and C···H as the major interactions towards crystal packing while π···π stacking and C-H···π interaction are responsible for extending the supramolecular network of the complex and stabilizing the crystal structure. The findings of Hirshfeld surface analysis are in consistent with the intermolecular interaction motifs obtained

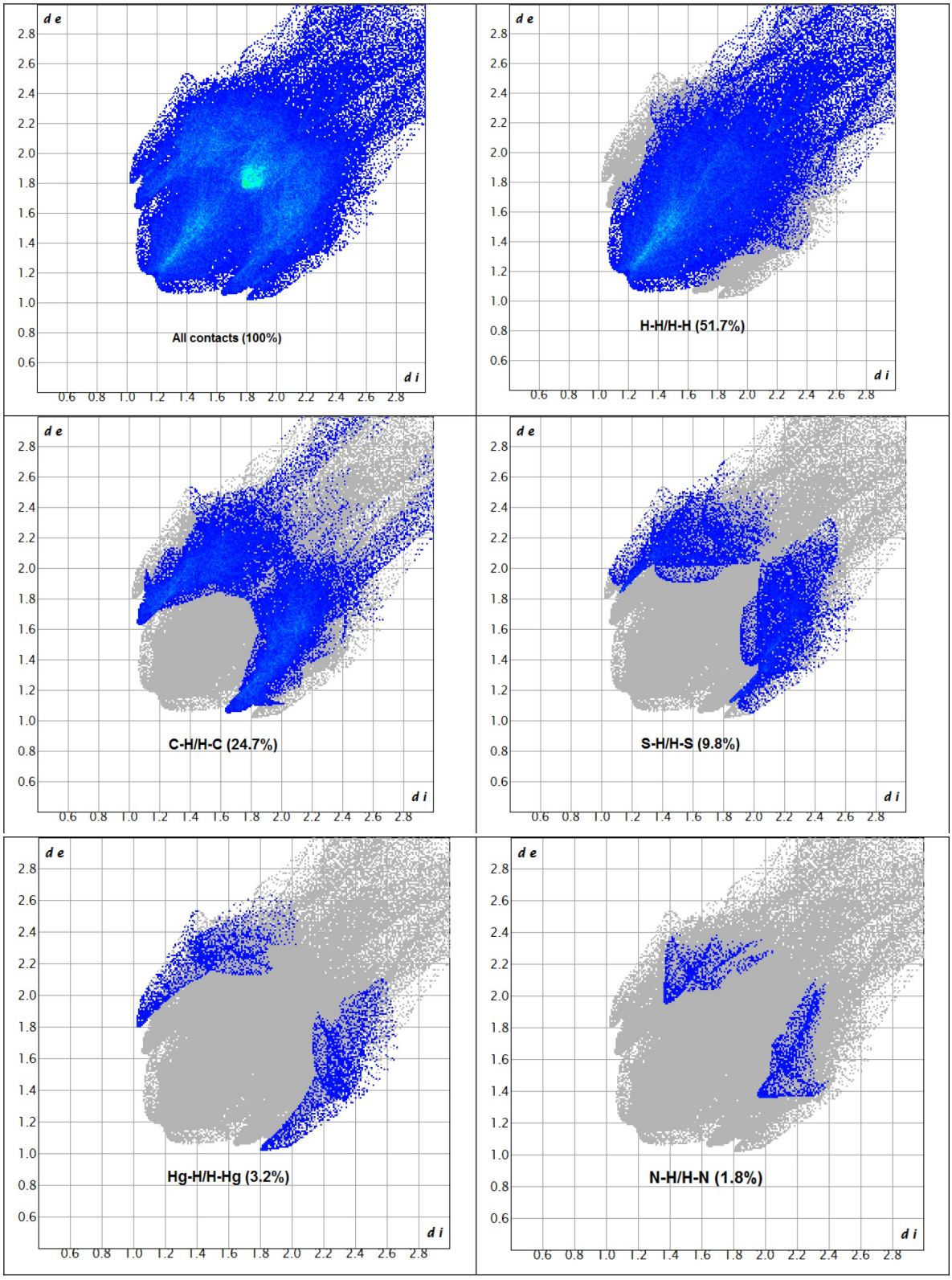

Figure 9. Two-dimensional fingerprint plot of the molecule showing the contributions of individual interactions.

from structural analysis. This type of Hg(II) based metal complex may further be studied for construction of coordination polymers and superstructures and their functional behaviours. The primary focuses of this study take account of the structural

elucidation of the pyrene-based Hg(II) complex with see-saw geometry which can be classified under exceptional category of metal complexes and exploration of the different types of weak interactions present within the crystal of this rare type of complex. We strongly believe that this work is highly relevant to the researchers in the field of molecular designing as well as crystal engineering.

4. Appendix A. Supplementary Data

CCDC 2325379 contains the supplementary crystallographic data for **1**. These data can be obtained free of charge *via* http://www.ccdc.cam.ac.uk/conts/retrieving.html, or from the Cambridge Crystallographic Data Centre, 12 Union Road, Cambridge CB2 1EZ, UK; fax: (+44) 1223–336-033; or e-mail: deposit@ccdc.cam.ac.uk.

Acknowledgements

The author Mohd Afzal extends his appreciation to the "Researchers Supporting Project number (RSPD2024R979)", King Saud University, Riyadh, Saudi Arabia for financial assistance.

Conflict of Interest

The authors declare that they have no known competing financial interests or personal relationships that could have appeared to influence the work reported in this paper.

Data Availability Statement

The data that support the findings of this study are available from the corresponding author upon reasonable request.

Keywords: Hg(II) · Crystal structure · Weak interactions · DFT · Hirshfeld surface

[1] R. Liu, W. Zhang, D. Wei, J.-H. Chen, S. W. Ng, G. Yang, *Dalton Trans.* **2019**, *48*, 16162–16166.
[2] S. Roy, M. G. B. Drew, A. Bauzá, A. Frontera, S. Chattopadhyay, *Dalton Trans.* **2017**, *46*, 5384–5397.
[3] J.-X. Li, Z.-X. Du, Q.-Y. Pan, L.-L. Zhang, D.-L. Liu, *Inorg. Chem.* **2020**, *509*, 119677.
[4] S. Mirdya, S. Roy, S. Chatterjee, A. Bauzá, A. Frontera, S. Chattopadhyay, *Cryst. Growth Des.* **2019**, *19*(10), 5869–5881.
[5] M. N. Ahmed, M. Madni, S. Anjum, S. Andleeb, S. Hameed, A. M. Khan, M. Ashfaq, M. N. Tahir, D. M. Gil, A. Frontera, *CrystEngComm* **2021**, *23*, 3276–3287.
[6] A. Singh, G. Kociok-Köhn, A. Dutta, A. Kumar, M. Muddassir, *J. Solid State Chem.* **2022**, *315*, 123517.
[7] G. Mahmoudi, E. Zangrando, B. Miroslaw, A. V. Gurbanov, M. G. Babashkina, A. Frontera, D. A. Safin, *Inorg. Chim. Acta* **2021**, *519*, 120279.
[8] G. Mahmoudi, A. Bauzá, A. V. Gurbanov, F. I. Zubkov, W. Maniukiewicz, A. Rodríguez-Diéguez, E. Lopez-Torres, A. Frontera, *CrystEngComm* **2016**, *18*(47), 9056–9066.
[9] G. Gervasio, D. Marabello, *Acta Crystallogr.* **2007**, *C63*, m318–m320.
[10] K. L. Jyothi, M. K. Hema, K. Kumara, T. G. Row, N. K. Lokanath, *J. Mol. Struct.* **2023**, *1280*, 135072.
[11] Z. Jabri, A. A. Thiruvalluvar, R. Sghyar, J. T. Mague, S. Sabir, Y. K. Rodi, E. H. Anouar, K. Misbahi, N. K. Sebbar, E. M. Essassi, *J. Biomol. Struct. Dyn.* **2023**, 1–16.
[12] M. Shellaiah, Y. C. Rajan, P. Baluc, A. Murugan, *New J. Chem.* **2015**, *39*, 2523–2531.
[13] Bruker, *SMART v5.631*, Bruker AXS Inc., Madison, WI, USA, **2001**.
[14] G. M. Sheldrick, *SHELXS-97, SHELXL-97*, University of Gőttingen, Gőttingen, Germany, **1997**.
[15] *Gaussian 16, Revision C.01*, M. J. Frisch, G. W. Trucks, H. B. Schlegel, G. E. Scuseria, M. A. Robb, J. R. Cheeseman, G. Scalmani, V. Barone, G. A. Petersson, H. Nakatsuji, X. Li, M. Caricato, A. V. Marenich, J. Bloino, B. G. Janesko, R. Gomperts, B. Mennucci, H. P. Hratchian, J. V. Ortiz, A. F. Izmaylov, J. L. Sonnenberg, D. Williams-Young, F. Ding, F. Lipparini, F. Egidi, J. Goings, B. Peng, A. Petrone, T. Henderson, D. Ranasinghe, V. G. Zakrzewski, J. Gao, N. Rega, G. Zheng, W. Liang, M. Hada, M. Ehara, K. Toyota, R. Fukuda, J. Hasegawa, M. Ishida, T. Nakajima, Y. Honda, O. Kitao, H. Nakai, T. Vreven, K. Throssell, J. A. Montgomery, Jr., J. E. Peralta, F. Ogliaro, M. J. Bearpark, J. J. Heyd, E. N. Brothers, K. N. Kudin, V. N. Staroverov, T. A. Keith, R. Kobayashi, J. Normand, K. Raghavachari, A. P. Rendell, J. C. Burant, S. S. Iyengar, J. Tomasi, M. Cossi, J. M. Millam, M. Klene, C. Adamo, R. Cammi, J. W. Ochterski, R. L. Martin, K. Morokuma, O. Farkas, J. B. Foresman,, D. J. Fox, Gaussian, Inc., Wallingford CT **2016**.
[16] R. Dennington, T. A. Keith, J. M. Millam, *GaussView, Version 6.0*; Semichem Inc., Shawnee Mission: Shawnee, Kansas **2016**.
[17] R. Krishnan, J. S. Binkley, R. Seeger, J. A. Pople, *J. Chem. Phys.* **1980**, *72*, 650–654.
[18] A. D. Becke, *J. Chem. Phys.* **1993**, *98*, 5648–5652.
[19] M. J. Turner, J. J. McKinnon, S. KWolff, D. J. Grimwood, P. R. Spackman, D. Jayatilaka, M. A. Spackman, *Crystal Explorer17*, University of Western Australia, **2017**.
[20] L. Yang, D. R. Powell, R. P. Houser, *Dalton Trans.* **2007**, *9*, 955–964.
[21] G. J. Grant, M. E. Botros, J. S. Hassler, D. E. Janzen, C. A. Grapperhaus, M. G. O'Toole, D. G. VanDerveer, *Polyhedron* **2008**, *27*, 3097–3104.
[22] M. Pinsky, D. Avnir, *Inorg. Chem.* **1998**, *37*, 5575–5582.
[23] S. Lakshminarayanan, V. Jeyasingh, K. Murugesan, N. Selvapalam, G. Dass, *J. Photochem. Photobiol.* **2021**, *6*, 100022.
[24] M. A. Spackman, J. Dylan, *CrystEngComm.* **2009**, *11*, 19–32.
[25] M. Guin, S. Halder, S. Chatterjee, S. Konar, *J. Mol. Struct.* **2022**, *1270*, 133949.
[26] A. De, M. A. Kathait, P. Jain, M. Guin, *ChemistrySelect* **2022**, *7*(42), e202202884.
[27] S. J. Munshi, M. Guin, S. Kundu, S. B. Kumar, *J. Indian Chem. Soc.* **2021**, *98*, 100080.
[28] M. Ashfaq, K. S. Munawar, M. N. Tahir, N. Dege, M. Yaman, S. Muhammad, S. S. Alarfaji, H. Kargar, M. U. Arshad, *ACS Omega* **2021**, *6*(34), 22357–22366.
[29] L. H. Al-Wahaibi, J. Joubert, O. Blacque, N. H. Al-Shaalan, A. A. El-Emam, *Sci. Rep.* **2019**, *9*, 19745.

Manuscript received: May 20, 2024
Revised manuscript received: July 22, 2024
Accepted manuscript online: July 29, 2024

RESEARCH ARTICLE

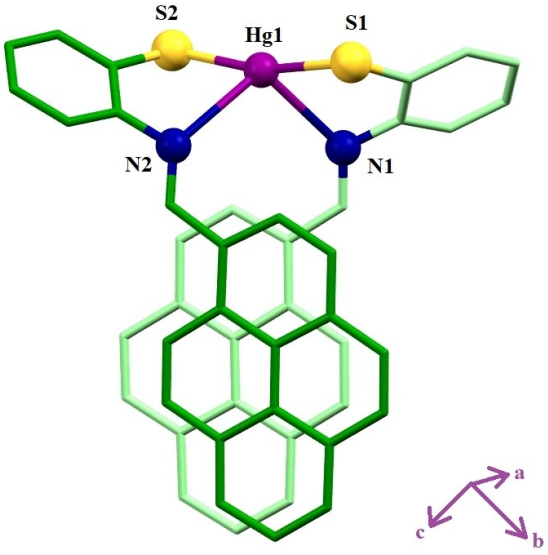

S. Halder, Y. Sikdar, M. Afzal, M. Guin, S. Konar**